5
Dynamics of deformed Hénon-like map

5.1 INTRODUCTION

The Hénon map was introduced in [Hénon, 1976] as a simplified model of the Poincare section of the Lorenz model. It is the first example of two-dimensional quadratic map for which a non-hyperbolic strange attractor shown numerically. The Hénon map exhibits the stretching and folding properties of the Poincare map. One of the differences between the Hénon system and Lorenz system is that some trajectories of the Hénon map escape to infinity, whereas the Lorenz system has all bounded trajectories.

An attractor is a compact invariant set Λ with a dense orbit and whose stable set has non-empty interior. If an attractor Λ has a dense orbit with a positive Lyapunov exponent, then it is called strange attractor. In [Benedicks and Carleson, 1991], it was proved that there exists a set of positive two-dimensional Lebesgue measure such that the Hénon family exhibits strange attractor, which is the closure of unstable manifold of the fixed point which lie in the first quadrant. These results have been extended in [Mora and Viana, 1993] to a more general perturbation of the quadratic family on the real line i.e. Hénon-like maps.

In this chapter, we apply the type-3 deformation on Hénon-like maps and obtain the deformed Hénon-like map, namely q-Hénon-like map. We investigate the various dynamical properties of q-Hénon maps for different deformed parameters. First we construct the "most attracting curve" in the parameter space, where the transition take place from simple to chaotic dynamics. On the boundary, these maps have special properties. The topological and geometrical properties of these maps are very interesting to study. We use heteroclinic web, it is the structure of stable and unstable manifolds of periodic points of q-Hénon maps and the concept of renormalization to describe the dynamics of q-Hénon-like maps. Finally, we conclude with some similarities and differences between the q-Hénon maps and the canonical Hénon maps.

This work is organized as follows. In Section 5.2, we discuss the formation of the q-Hénon map by applying the deformation on the state variable x. We discuss some basic properties and stability of the fixed points of the system. In Section 5.3, we propose an algorithm for the construction of a curve of parameter (a,b) such that the q-Hénon map on this curve has an attracting period 2^n-cycles (as $n \to \infty$). These curves are denoted by $\gamma_{2^\infty,\varepsilon}$ for each ε associated to the deformed parameter q. We show that for $\varepsilon > 0$, the phase transition happens prior to the canonical Hénon-like maps, which explains the Parrondo's paradoxical behaviour. We also describe the location of periodic attractors by tracing the unstable manifold of the fixed points. In Section 5.4, we define the heteroclinic web and describe the heteroclinic bifurcation on the curve $\gamma_{2^\infty,\varepsilon}$ for various ε values. Further, we show that before the heteroclinic bifurcation on the curve $\gamma_{2^\infty,\varepsilon}$, all q-Hénon maps are infinitely renormalizable and having Cantor set as an attractor. Finally in Section 5.5, we show that the basin of attraction of q-Hénon maps do not have an escaping region for a particular set of deformed parameters.

5.2 Q-DEFORMATION OF HÉNON-LIKE MAPS

The Hénon-like map is given by the following system

$$\begin{aligned} x_{n+1} &= f_a(x_n) - by_n \\ y_{n+1} &= x_n \end{aligned} \tag{5.1}$$

where $a \geq 1$ and $b > 0$ are the parameters. The Hénon-like map is an area contracting map if $|b| < 1$ and it is area preserving map when $b = 1$. Note that the map has constant determinant of Jacobian b and it is orientation preserving map for $b > 0$.

The Hénon-like map corresponding to the system (5.1) can be re-written as

$$H_{a,b}\begin{pmatrix} x \\ y \end{pmatrix} = \begin{pmatrix} f_a(x) - by \\ x \end{pmatrix} \tag{5.2}$$

where $0 \leq b < 1$ and $f_a(x) = a - x^2$. In the case of degenerate map ($b = 0$), there exist a unique a^* for which the map $H_{a^*,0}$ is the accumulation of period doubling.

In the non-extensive statistical mechanics of Tsallis [Gell-Mann and Tsallis, 2004], the deformation of real number x has been introduced as

$$[x]_q = \frac{x}{1 + (1-x)(1-q)}. \tag{5.3}$$

As the deformed parameter $q \to 1$, then the deformed number $[x]_q \to x$.

Let $1 - q = \varepsilon$, then Eq. (5.3) can be rewritten as

$$[x]_\varepsilon = \frac{x}{1 + \varepsilon(1-x)}, \tag{5.4}$$

where $\varepsilon \in (-1, \infty)$. For computational purpose we consider $\varepsilon \in [-0.2, 0.5]$ in our discussion. Clearly, $[x]_\varepsilon$ and inverse of $[x]_\varepsilon$ are continuous on $x \in (-2, 3)$. Therefore, the deformation map $[x]_\varepsilon$ is a homeomorphism for $x \in (-2, 3)$.

The second equation of Hénon-like map (5.1) indicates that y_{n+1} states are the previous x_n states. So the information about dynamic action found entirely in the sequence x_n alone. This suggest that it is meaningful to analyze the deformation on state variable x_n only. Therefore, we apply the deformation $[x]_\varepsilon$ in the direction of state variable x of Hénon-like map Eq. (5.2). Then we obtain the deformed Hénon-like map as

$$H_{a,b}\begin{pmatrix} [x]_\varepsilon \\ y \end{pmatrix} = \begin{pmatrix} f_a([x]_\varepsilon) - by \\ [x]_\varepsilon \end{pmatrix} \equiv \mathscr{H}_{a,b,\varepsilon}\begin{pmatrix} x \\ y \end{pmatrix} \tag{5.5}$$

On simplification, we get

$$\mathscr{H}_{a,b,\varepsilon}\begin{pmatrix} x \\ y \end{pmatrix} = \begin{pmatrix} F_{a,\varepsilon}(x) - by \\ \frac{x}{1+\varepsilon-\varepsilon x}. \end{pmatrix} \tag{5.6}$$

where

$$F_{a,\varepsilon}(x) = a - \frac{x^2}{(1+\varepsilon-\varepsilon x)^2}, \ 0 \leq b \leq 1, \text{ and } a > 0.$$

Here, the map $F_{a,\varepsilon}(x)$ is a q-deformed one-dimensional map. As the parameter $\varepsilon \to 0$, the map $F_{a,\varepsilon}(x)$ approaches to the quadratic map $f_a(x)$.

Note that for $\varepsilon = 0$, the map $\mathscr{H}_{a,b,\varepsilon}$ reduces to the canonical Hénon-like map $H_{a,b}$. For the convenience of notation we use $\mathscr{H}$ instead of $\mathscr{H}_{a,b,\varepsilon}$.

5.2.1 Basic properties

(i) The q-Hénon map $\mathscr{H}$ is obtained by the composition of the following transformations:

$$\mathscr{H}_1\begin{pmatrix}x\\y\end{pmatrix}=\begin{pmatrix}\frac{x}{(1+\varepsilon-\varepsilon x)}\\y\end{pmatrix},\ \mathscr{H}_2\begin{pmatrix}x\\y\end{pmatrix}=\begin{pmatrix}x\\k_1-k_2x^2-y\end{pmatrix},$$
$$\mathscr{H}_3\begin{pmatrix}x\\y\end{pmatrix}=\begin{pmatrix}x\\by\end{pmatrix},\qquad \mathscr{H}_4\begin{pmatrix}x\\y\end{pmatrix}=\begin{pmatrix}y\\x\end{pmatrix},$$

where the constants $k_1=b/a$ and $k_2=1/b$, such that

$$\mathscr{H}\begin{pmatrix}x\\y\end{pmatrix}=\mathscr{H}_4\circ\mathscr{H}_3\circ\mathscr{H}_2\circ\mathscr{H}_1\begin{pmatrix}x\\y\end{pmatrix}.$$

(ii) The q-Hénon map $\mathscr{H}$ is injective and the inverse is $\mathscr{H}^{-1}\begin{pmatrix}x\\y\end{pmatrix}=\begin{pmatrix}\frac{(1+\varepsilon)y}{1+\varepsilon y}\\\frac{a-y^2-x}{b}\end{pmatrix}$.

(iii) The determinant of the Jacobian $J(\mathscr{H})$ of q-Hénon map is non-constant and the eigenvalues of the Jacobian are real if $b\leq\frac{x^2(1+\varepsilon)}{(1+\varepsilon-\varepsilon x)^4}$.

Proof. The Jacobian of the q-Hénon map is given by

$$J(\mathscr{H})\begin{pmatrix}x\\y\end{pmatrix}=\begin{pmatrix}\frac{-2x(1+\varepsilon)}{(1+\varepsilon-x\varepsilon)^3} & -b\\ \frac{(1+\varepsilon)}{(1+\varepsilon-x\varepsilon)^2} & 0\end{pmatrix} \tag{5.7}$$

The $det\,J(\mathscr{H})(x,y)=\frac{b(1+\varepsilon)}{(1+\varepsilon-\varepsilon x)^2}$ which varies w.r.t. the values of b,ε and x.

We solve $det\,(J(\mathscr{H})-\xi I)=0$ for ξ to calculate the eigenvalue of matrix $J(\mathscr{H})$, where I is the identity matrix of order 2. Then we get

$$\xi^2+\frac{2x(1+\varepsilon)}{(1+\varepsilon-\varepsilon x)^3}\xi+\frac{b(1+\varepsilon)}{(1+\varepsilon-\varepsilon x)^2}=0.$$

Solving, we obtain

$$\xi=\frac{-(1+\varepsilon x)}{(1+\varepsilon-\varepsilon x)^2}\pm\frac{1}{2(1+\varepsilon-\varepsilon x)^3}\sqrt{x^2(1+\varepsilon)^2-b(1+\varepsilon-\varepsilon x)^4}$$

which is real if $b\leq\frac{x^2(1+\varepsilon)}{(1+\varepsilon-\varepsilon x)^4}$. □

5.2.2 Fixed points of q-Hénon map

To calculate the fixed points, we solve the system

$$\mathscr{H}\begin{pmatrix}x\\y\end{pmatrix}=\begin{pmatrix}x\\y\end{pmatrix},$$

which yields the following system of equations:

$$a-\frac{x^2}{(1+\varepsilon-\varepsilon x)^2}-by=x \tag{5.8}$$

$$\frac{x}{1+\varepsilon-\varepsilon x} = y \tag{5.9}$$

From the above Eqs. (5.8) and (5.9), we obtain

$$\varepsilon y^3 + (1+b\varepsilon)y^2 + (1+b+\varepsilon-a\varepsilon)y - a = 0. \tag{5.10}$$

For each $\varepsilon \neq 0$, the above cubic polynomial has three roots for y which can be real or imaginary depending on value of ε. Once we have the value of y, then we get the fixed point (x,y) by Eq. (5.9). For $\varepsilon = 0$, the Eq. (5.10) has two roots which yields to the fixed points corresponding to the canonical Hénon map $H_{a,b}$.

Let $\mathscr{D}_\varepsilon = (-0.2,0)\cup(0,0.5)$. Now we analyze the existence of fixed points of q-Hénon map for each $\varepsilon \in \mathscr{D}_\varepsilon$. For the initial values of ε, we see that there are three fixed points, out of which one is stable α_1 (say), one is flip saddle α_2 (say) and other one is regular saddle α_3 (say). Further, as the parameter ε varies, we observe that the stable fixed point coincide with regular saddle point and consequently disappears. It implies that the bifurcation occurs at some parameter ε_*. Notice that, when $\varepsilon > \varepsilon_*$, there is only one fixed point which is flip saddle α_2. For a particular parameters $a = 1$, and $b = 0.04999999$ by using numerical simulations we obtain the value of $\varepsilon_* = 0.1827$. It is illustrated in Fig. 5.1 by showing ε verses $y-$ coordinate of fixed points. Let $\mathscr{D}_\varepsilon^* = (-0.2,\varepsilon_*)\setminus\{0\}$, be the domain of parameters where the map has three fixed points. For a given $a = 1$ and each $b \in (0,0.5)$, we have computed ε_*, which are shown in Fig. 5.2.

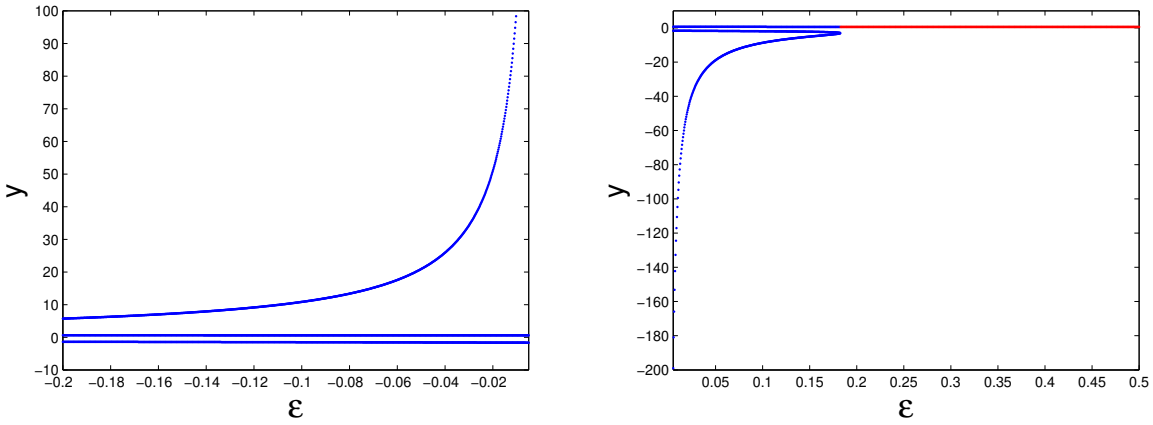

(i) (ii)

Figure 5.1. : The $y-$coordinates of the fixed points of $\mathscr{H}_{a,b,\varepsilon}$ at $a = 1$, $b = 0.04999999$. (i) for $\varepsilon \in (-0.2,-0.005)$; (ii) for $\varepsilon \in (0.005,0.5)$.

5.3 Q-HÉNON CYCLES

5.3.1 Construction of the 2^n-periodic points

We propose a method to construct superstable periodic points of period 2^n of the map $\mathscr{H}_{a,b,\varepsilon}$ in the parameter plane (a,b) for a given deformed parameter ε.
Method: Consider the q-Hénon map given by the Eq. (5.6),

$$\mathscr{H}_{a,b,\varepsilon}(x,y) = \left(F_{a,\varepsilon}(x) - by, \frac{x}{1+\varepsilon-\varepsilon x}\right) \tag{5.11}$$

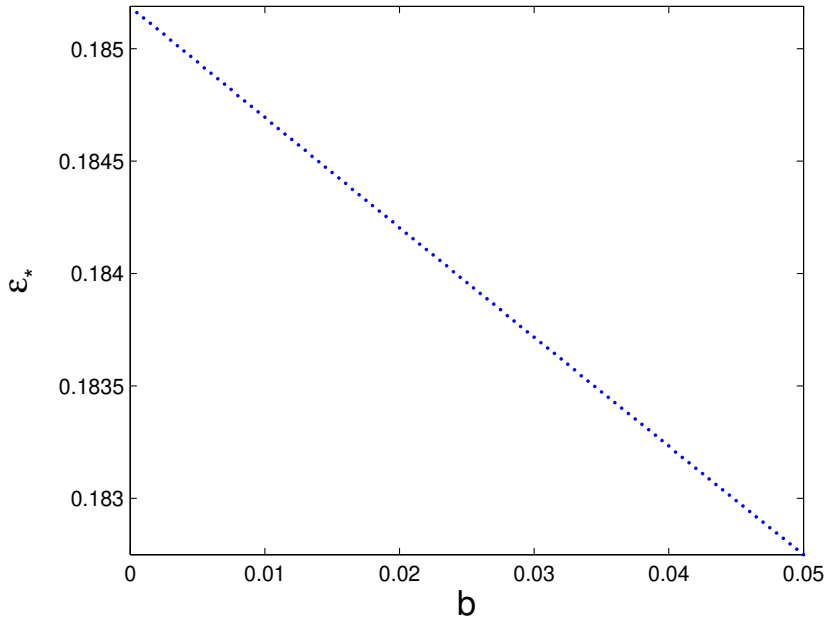

Figure 5.2. : The value of ε_* for each value of $b \in (0, 0.05)$ at $a = 1$.

where $F_{a,\varepsilon}(x) = a - \frac{x^2}{(1+\varepsilon-\varepsilon x)^2}$ and $0 \leq b \leq 1$, $a > 0$.

For $b = 0$ and given $\varepsilon \in \mathscr{D}_\varepsilon$, the map $\mathscr{H}_{a,b,\varepsilon}$ reduces to the degenerate q-Hénon map $\mathscr{H}_{a,0,\varepsilon}$. Note that $F_{a,\varepsilon}(x)$ is an unimodal map with unique critical point at $x = 0$. One can easily compute the sequence of parameters

$$\{a_0^{2^1}, a_0^{2^2}, a_0^{2^3}, \ldots, a_0^{2^n} \ldots\}$$

at which the map $F_{a,\varepsilon}(x)$ has 2^n-superstable periodic points. In general, a periodic point is superstable if and only if the critical point of the map belongs to that periodic cycle. Therefore, we obtain the sequence $\{a_0^{2^n}\}$ by solving the following polynomial

$$F_{a,\varepsilon}^{2^n}(0) = 0$$

for parameter a at fixed ε, where $n = 1, 2, \ldots$. Clearly this sequence $\{a_0^{2^n}\}$ converges to some a_0^*, at which the degenerate q-Hénon map undergoes the accumulation of period doubling. We have computed the parameter values 'a' for different ε by solving the equation $F_{a,\varepsilon}^{2^n}(0) = 0$ numerically using the MATLAB software. The sequence $a_0^{2^n}$ and corresponding Feigenbaum ratios for various ε are given in Table D.1 of Appendix D. We can observe that the sequence of parameters $a_0^{2^n}$ converges to $4.669201\ldots$.

The next step is to vary the parameter b as $b_{i+1} = b_i + \delta$ with $\delta = 10^{-9}$, and then compute the superstable periodic points of the map $\mathscr{H}(x, y)$. This means, for each b_i we have a vector $v_i^{2^n} = (x_i^{2^n}, y_i^{2^n}, a_i^{2^n})$ in such a way that $(x_i^{2^n}, y_i^{2^n})$ is a periodic point of period 2^n at the parameters $(a_i^{2^n}, b_i)$, and the trace of the Jacobian of $(2^n)^{\text{th}}$ iteration of the map $\mathscr{H}$ is equal to 0. This leads to the following equations:

$$\mathscr{H}^{2^n}\begin{pmatrix} x \\ y \end{pmatrix} - \begin{pmatrix} x \\ y \end{pmatrix} = 0 \tag{5.12}$$

$$Tr\,J\left(\mathscr{H}^{2^n}\begin{pmatrix}x\\y\end{pmatrix}\right)=0 \tag{5.13}$$

Let $X^0=x, Y^0=y$ and $(X^k,Y^k)=\mathscr{H}^k(x,y)$.
For $k\geq 0$, (X^{k+1},Y^{k+1}) can be written explicitly as function of x,y and a. Then we have

$$\begin{pmatrix}X^{k+1}\\Y^{k+1}\end{pmatrix}=\begin{pmatrix}a-\frac{(X^k)^2}{(1+\varepsilon-\varepsilon X^k)^2}-bY^k\\ \frac{X^k}{1+\varepsilon-\varepsilon X^k}\end{pmatrix} \tag{5.14}$$

We denote the partial derivatives of X^k as

$$X^k_x=\frac{\partial X^k}{\partial x},\ X^k_y=\frac{\partial X^k}{\partial y},\ X^k_a=\frac{\partial X^k}{\partial a},$$

and the second partial derivatives as

$$X^k_{xx},\ X^k_{xy},\ X^k_{xa},\ X^k_{yx},\ X^k_{yy},\ X^k_{ya}.$$

The Jacobian J for the first iteration $(X^1,Y^1)=\mathscr{H}(X^0,Y^0)$ is

$$J(X^0,Y^0)=\begin{pmatrix}\frac{-2(1+\varepsilon)X^0}{(1+\varepsilon-\varepsilon X^0)^3} & -b\\ \frac{(1+\varepsilon)}{(1+\varepsilon-\varepsilon X^0)^2} & 0\end{pmatrix}=\begin{pmatrix}K_1 & L_1\\ M_1 & N_1\end{pmatrix} \tag{5.15}$$

The Jacobian J for the second iteration $(X^2,Y^2)=\mathscr{H}^2(X^0,Y^0)$ is

$$J^2(X^0,Y^0)=J(X^1,Y^1)\times J(X^0,Y^0),$$

$$\begin{aligned}J^2(X^0,Y^0)&=\begin{pmatrix}\frac{-2(1+\varepsilon)X^1}{(1+\varepsilon-\varepsilon X^1)^3} & -b\\ \frac{(1+\varepsilon)}{(1+\varepsilon-\varepsilon X^1)^2} & 0\end{pmatrix}\begin{pmatrix}K_1 & L_1\\ M_1 & N_1\end{pmatrix}\\&=\begin{pmatrix}\frac{-2(1+\varepsilon)X^1}{(1+\varepsilon-\varepsilon X^1)^3}K_1-bM_1 & \frac{-2(1+\varepsilon)X^1}{(1+\varepsilon-\varepsilon X^1)^3}L_1-bN_1\\ \frac{(1+\varepsilon)}{(1+\varepsilon-\varepsilon X^1)^2}K_1 & \frac{(1+\varepsilon)}{(1+\varepsilon-\varepsilon X^1)^2}L_1\end{pmatrix}=\begin{pmatrix}K_2 & L_2\\ M_2 & N_2\end{pmatrix}.\end{aligned}$$

Continuing in this way, we get the Jacobian J for m^{th} iteration $(X^m,Y^m)=\mathscr{H}^m(X^0,Y^0)$ is

$$J^m(X^0,Y^0)=\prod_{i=0}^{m-1}J(X^i,Y^i)=\begin{pmatrix}K_m & L_m\\ M_m & N_m\end{pmatrix},$$

where

$$\begin{pmatrix}K_m & L_m\\ M_m & N_m\end{pmatrix}=\begin{pmatrix}\frac{-2(1+\varepsilon)X^{m-1}}{(1+\varepsilon-\varepsilon X^{m-1})^3}K_{m-1}-bM_{m-1} & \frac{-2(1+\varepsilon)X^{m-1}}{(1+\varepsilon-\varepsilon X^{m-1})^3}L_{m-1}-bN_{m-1}\\ \frac{(1+\varepsilon)}{(1+\varepsilon-\varepsilon X^{m-1})^2}K_{m-1} & \frac{(1+\varepsilon)}{(1+\varepsilon-\varepsilon X^{m-1})^2}L_{m-1}\end{pmatrix}.$$

The trace of the Jacobian $J(\mathscr{H}^m)$ is given by

$$K_m+N_m=\frac{-2(1+\varepsilon)X^{m-1}}{(1+\varepsilon-\varepsilon X^{m-1})^3}K_{m-1}-bM_{m-1}+\frac{(1+\varepsilon)}{(1+\varepsilon-\varepsilon X^{m-1})^2}L_{m-1} \tag{5.16}$$

Now rewrite the Eq. (5.12) as ϕ_1, ϕ_2 and Eq. (5.13) as ϕ_3. Then we get

$$\begin{aligned}
\phi_1 &\equiv X^{2^n} - X^0 = 0 \\
&\equiv a - \frac{(X^{2^n-1})^2}{\lambda^2} - bY^{2^n-1} - X^0 = 0 \\
\phi_2 &\equiv Y^{2^n} - Y^0 = 0 \\
&\equiv \frac{X^{2^n-1}}{\lambda} - Y^0 = 0 \\
\phi_3 &\equiv X_x^{2^n} + Y_y^{2^n} = 0 \\
&\equiv \frac{-2(1+\varepsilon)X^{2^n-1}X_x^{2^n-1}}{\lambda^3} - bY_x^{2^n-1} + \frac{(1+\varepsilon)X_y^{2^n-1}}{\lambda^2} = 0
\end{aligned} \tag{5.17}$$

where $\lambda = 1+\varepsilon-\varepsilon X^{2^n-1}$. Now, we solve the above equations by employing the Newton algorithm. Let $v_i^{2^n}(t) = (x_i^{2^n}, y_i^{2^n}, a_i^{2^n})$ be the initial vector such that $(x_i^{2^n}, y_i^{2^n})$ is a periodic point of period 2^n with parameter $a_i^{2^n}$. Then the updated vector $v_i^{2^n}(t+1)$ is given by

$$v_i^{2^n}(t+1) = v_i^{2^n}(t) - \left((J(\phi))^{-1} \cdot \phi(v_i^{2^n}(t)) \right) \tag{5.18}$$

where

$$\phi = \begin{pmatrix} \phi_1 \\ \phi_2 \\ \phi_3 \end{pmatrix} \quad \text{and} \quad J(\phi) = \begin{pmatrix} \phi_{1x} & \phi_{1y} & \phi_{1a} \\ \phi_{2x} & \phi_{2y} & \phi_{2a} \\ \phi_{3x} & \phi_{3y} & \phi_{3a} \end{pmatrix}. \tag{5.19}$$

Computation of $J(\phi)$ will involve not only the first partial derivative but also the second partial derivatives of $\left(X^{2^n}, Y^{2^n}\right)$. We calculate these derivatives recursively. Thus, we have

$$\begin{aligned}
\phi_{1x} &= \frac{-2(1+\varepsilon)X^{2^n-1}X_x^{2^n-1}}{\lambda^3} - bY_x^{2^n-1} - 1, \\
\phi_{1y} &= \frac{-2(1+\varepsilon)X^{2^n-1}X_y^{2^n-1}}{\lambda^3} - bY_y^{2^n-1}, \\
\phi_{1a} &= \frac{-2(1+\varepsilon)X^{2^n-1}X_a^{2^n-1}}{\lambda^3} - bY_a^{2^n-1}, \\
\phi_{2x} &= \frac{(1+\varepsilon)X_x^{2^n-1}}{\lambda^2}, \\
\phi_{2y} &= \frac{(1+\varepsilon)X_y^{2^n-1}}{\lambda^2} - 1, \\
\phi_{2a} &= \frac{(1+\varepsilon)X_a^{2^n-1}}{\lambda^2}, \\
\phi_{3x} &= \frac{-2(1+\varepsilon)^2\left\{(X_x^{2^n-1})^2 + X^{2^n-1}X_{xx}^{2^n-1}\right\}}{\lambda^4} \\
&\quad + \frac{2\varepsilon(1+\varepsilon)\left\{(X^{2^n-1})^2X_{xx}^{2^n-1} - 2X^{2^n-1}(X_x^{2^n-1})^2\right\}}{\lambda^4} \\
&\quad + \frac{(1+\varepsilon)\left\{\lambda X_{xy}^{2^n-1} + 2\varepsilon X_x^{2^n-1}X_y^{2^n-1}\right\}}{\lambda^3} - bY_{xx}^{2^n-1}, \\
\phi_{3y} &= \frac{-2(1+\varepsilon)^2\left\{X_x^{2^n-1}X_y^{2^n-1} + X^{2^n-1}X_{yx}^{2^n-1}\right\}}{\lambda^4} \\
&\quad + \frac{2\varepsilon(1+\varepsilon)\left\{(X^{2^n-1})^2X_{yx}^{2^n-1} - 2X^{2^n-1}X_x^{2^n-1}X_y^{2^n-1}\right\}}{\lambda^4} \\
&\quad + \frac{(1+\varepsilon)\left\{\lambda X_{yy}^{2^n-1} + 2\varepsilon(X_y^{2^n-1})^2\right\}}{\lambda^3} - bY_{yx}^{2^n-1},
\end{aligned}$$

$$\phi_{3a} = \frac{-2(1+\varepsilon)^2\{X_x^{2^n-1}X_a^{2^n-1} + X^{2^n-1}X_{ax}^{2^n-1}\}}{\lambda^4} + \frac{2\varepsilon(1+\varepsilon)\{(X^{2^n-1})^2X_{ax}^{2^n-1} - 2X^{2^n-1}X_x^{2^n-1}X_a^{2^n-1}\}}{\lambda^4} + \frac{(1+\varepsilon)\{\lambda X_{ay}^{2^n-1} + 2\varepsilon X_a^{2^n-1}X_y^{2^n-1}\}}{\lambda^3} - bY_{ax}^{2^n-1}.$$

After the calculation of the above derivatives, we use the Eq. (5.18) to obtain the modified vector $v_i^{2^n}(t+1)$. Repeat this process until we get an accuracy 10^{-12} with the error term $e_i^{2^n} = v_i^{2^n}(t+1) - v_i^{2^n}(t) \leq 10^{-12}$ at which one can obtain optimal vector $v_{i+1}^{2^n}$. Let $w_i^{2^n} = v_{i+1}^{2^n}$ be the final modified vector obtained from the above method. Then $w_i^{2^n}$ serves as initial vector for the next increment $b_{i+1} = b_i + \delta$. If we consider the initial vector within the basin of attraction of the period 2^n orbit, one can easily find the orbit by repeated iterations. Then gradually change b_i to $b_i + \delta$ with increment δ and compute the corresponding parameter $a_{i+1}^{2^n}$ using the above Newton algorithm. For a given ε and for each $b_i \in (0, 0.05)$, we calculate corresponding a_i value such that the parameters (a_i, b_i) forms a short curve in the parameter space (a,b). This curve is called as "most attracting" curve. For different ε, these curves are denoted by $\gamma_{2^n,\varepsilon}$.

Next, we describe the above method as a computational algorithm for the calculation of 2^n-superstable periodic points of q-Hénon map in the following steps::

(1) First, fix the parameter ε, period $P = 2^n$ (for $n = 0, 1, \ldots$) and the tolerance error E.

(2) Consider initial value as $(x_0, y_0) = (0,0)$ and calculate a_0 corresponding to $b_0 = 0$ by solving $F_{a,\varepsilon}^{2^n}(0) = 0$ for parameter a.

(3) Consider b_i, start from $i = 0$.

(4) The initial vector is $v_i(t) = (x_i, y_i, a_i)$ for b_i.

(5) Take $X^0 = x_i$, $Y^0 = y_i$, $a = a_i$, and iterate $\mathscr{H}$ by P times to get X^{2^n} and Y^{2^n}. Use these values to calculate ϕ_1 and ϕ_2.

(6) Calculate the trace of the Jacobian $J(\mathscr{H}^m(x,y))$ using Eq. (5.16) at $m = 2^n$, where K_1 and L_1 are given by the Eq. (5.15). From this we obtain ϕ_3 and formulate the vector $\phi = (\phi_1, \phi_2, \phi_3)^t$.

(7) Compute the matrix $J(\phi)$ using the partial derivatives, and evaluate inverse of $J(\phi)$.

(8) Calculate the updated vector $v_i(t+1) = v_i(t) - \big((J(\phi))^{-1} \cdot \phi(v_i(t))\big)$.

(9) If $| v_i(t+1) - v_i(t) | \leq E$ then $w_i(t) = (x_i^*, y_i^*, a_i^*)$, otherwise go to step (5).

(10) For next increment of i, $b_i = b_{i-1} + \delta$.

(11) Use $v_i(t) = w_i(t)$ as the initial vector for b_i, and go to step (4). Then repeat the steps from (4) to (9) until we obtain the optimal vector $w_i(t) = (x_i^*, y_i^*, a_i^*)$ corresponding to b_i.

We have implemented this algorithm by using C program, and taking $E = 10^{-12}$ and $\delta = 10^{-9}$. The curves $\gamma_{2^n,\varepsilon}$ are shown in Fig. 5.3 for the period 2^{11}, by considering various ε values. We observe that as ε increasing from -0.2 to 0.5 then the curves $\gamma_{2^n,\varepsilon}$ are shifting from the right to left side on the parameter a scale. The parameters (a,b) on this curve $\gamma_{2^n,\varepsilon}$ leads to a particular q-Hénon map which has the superstable periodic orbits of period 2^n. The accuracy of computations are verified by calculating the difference between Feigenbaum ratio for the sequence of parameters $a_i^{2^n}$ to the actual Feigenbaum constant ($\delta = 4.669201609\ldots$), which are shown in Table 5.1, for $b = 0.04999999$ and $\varepsilon \in (-0.2, 0.5)$. Note that, as $n \to \infty$, the curves $\gamma_{2^n,\varepsilon}$ converges to the Feigenbaum map $\gamma_{2^\infty,\varepsilon}$

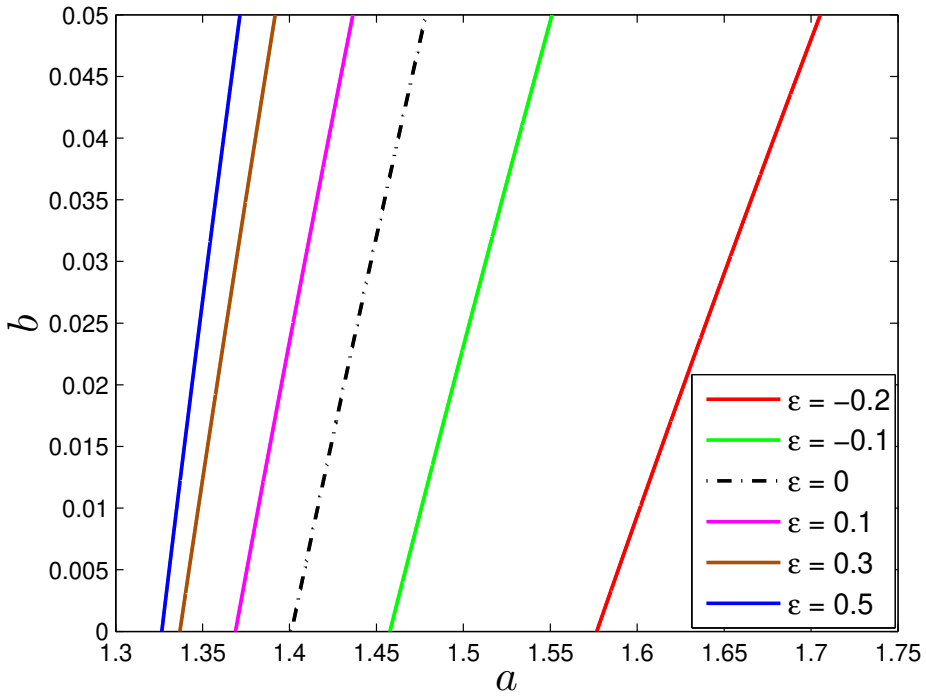

Figure 5.3. : Superstable periodic point of period 2^{11} for different values of ε.

which are shown here as an approximation of $\gamma_{2^n,\varepsilon}$, $(n \approx 11)$. On this approximated curve $\gamma_{2^n,\varepsilon}$ the q-Hénon maps undergoes a transition from periodic to chaotic behaviour. The attracting periodic orbit disappears and obtain chaos for the value of parameter (a,b) that are lies on the right side of the curve $\gamma_{2^n,\varepsilon}$.

Period $\rightarrow$	2^9	2^{10}	2^{11}
$\varepsilon = -0.2$	$8.5*10^{-5}$	$1.8*10^{-5}$	$3.9*10^{-6}$
$\varepsilon = -0.1$	$4.2*10^{-5}$	$9.1*10^{-6}$	$1.8*10^{-6}$
$\varepsilon = 0$	$2.9*10^{-5}$	$6.3*10^{-6}$	$1.3*10^{-6}$
$\varepsilon = 0.1$	$2.5*10^{-5}$	$5.4*10^{-6}$	$1.1*10^{-6}$
$\varepsilon = 0.2$	$2.4*10^{-5}$	$5.2*10^{-6}$	$1.1*10^{-6}$
$\varepsilon = 0.3$	$2.5*10^{-5}$	$5.4*10^{-6}$	$1.2*10^{-6}$
$\varepsilon = 0.5$	$3.4*10^{-5}$	$7.2*10^{-6}$	$1.5*10^{-6}$

Table 5.1. : Accuracy of calculated Feigenbaum ratio to the actual Feigenbaum constant at $b = 0.04999999$.

Let $W_{|\varepsilon_1,\varepsilon_2|}$ be the bounded domain between the curves $\gamma_{2^\infty,\varepsilon_1}$ and $\gamma_{2^\infty,\varepsilon_2}$, where $\varepsilon_1, \varepsilon_2 \in (-0.2, 0.5)$, and $\varepsilon_1 > \varepsilon_2$. Let $\mathscr{H}_{a,b,\varepsilon}$ be a q-Hénon map such that the parameters a, b, ε lies within the bounded domain $W_{|\varepsilon_1,\varepsilon_2|}$. Clearly, the map $\mathscr{H}_{a,b,\varepsilon}$ exhibit periodic behaviour for $\varepsilon = \varepsilon_2$ and it exhibit chaotic behaviour for $\varepsilon = \varepsilon_1$. In particular, if any map $\mathscr{H}_{a,b,\varepsilon}$ within the domain $W_{|-0.1,-0.2|}$, which is bounded by the curves $\gamma_{2^\infty,-0.1}$ and $\gamma_{2^\infty,-0.2}$, then the map $\mathscr{H}_{a,b,\varepsilon}$ has periodic behaviour w.r.t. $\varepsilon = -0.2$, while the map has chaotic dynamics w.r.t. $\varepsilon = -0.1$. Therefore, as the value of ε increases, the chaotic part of the q-Hénon map $\mathscr{H}_{a,b,\varepsilon}$ increases. For $\varepsilon > 0$, we obtain the chaos for

parameter a which is prior to a^* of canonical Hénon-like map $H_{a,b}$.

The Hénon-like map $H_{a,b}(x)$ has simple dynamics for the parameter 'a' prior to the curve $\gamma_{2^\infty,0}$. The deformation map $[x]_\varepsilon$ is given by the Eq. (5.4) is a homeomorphism and hence it has a simple dynamics. But, the composition $H_{a,b} \circ [x]_\varepsilon$ which is q-Hénon map $\mathscr{H}_{a,b,\varepsilon}$, has a chaotic dynamics for the parameter a prior to the curve $\gamma_{2^\infty,0}$, whenever $\varepsilon > 0$. This is similar to the paradox observed in [Cánovas and Muñoz-Guillermo, 2019] for the deformed one-dimensional map. Therefore, we conclude that the above discussion leads to the existence of Parrondo's Paradox in q-Hénon maps.

5.3.2 Location of periodic attractors on $\gamma_{2^n,\varepsilon}$ of the q-Hénon map

We analyze the location of periodic attractors of the map $\mathscr{H}_{a,b,\varepsilon}$ on the curve $\gamma_{2^n,\varepsilon}$, where $\varepsilon \in \mathscr{D}_\varepsilon^* \cup (\varepsilon_*, 0.5) \cup \{0\}$.

Case (i): When $\varepsilon \in \mathscr{D}_\varepsilon^* = (-0.2, 0) \cup (0, \varepsilon_*)$, the map $\mathscr{H}_{a,b,\varepsilon}$ has three fixed points, in which α_1 is stable and it is coexists with flip saddle α_2 and regular saddle α_3. To illustrate the location of periodic points, we choose $\varepsilon = -0.1$ and $\varepsilon = 0.1$ and plotted the periodic attractors, which are depicted in Fig. 5.4 and Fig. 5.5 respectively. The zoom part around α_2 are shown in Fig. 5.4(ii) and Fig. 5.5(ii). Notice that all periodic points of period 2^{11} exists near to the flip saddle α_2.

Case (ii): When $\varepsilon \in (\varepsilon_*, 0.5)$, the situation is very different from the previous case as α_1 and α_3 disappears and now the map has only one fixed point α_2. This case is shown in Fig. 5.6 by taking $\varepsilon = 0.3$, and observe that the periodic orbits of period 2^{11} exists near the fixed point α_2.

Case (iii): When $\varepsilon = 0$, the q-Hénon map reduces to the canonical Hénon-like map, and there are only two fixed points; α_2 and α_3.

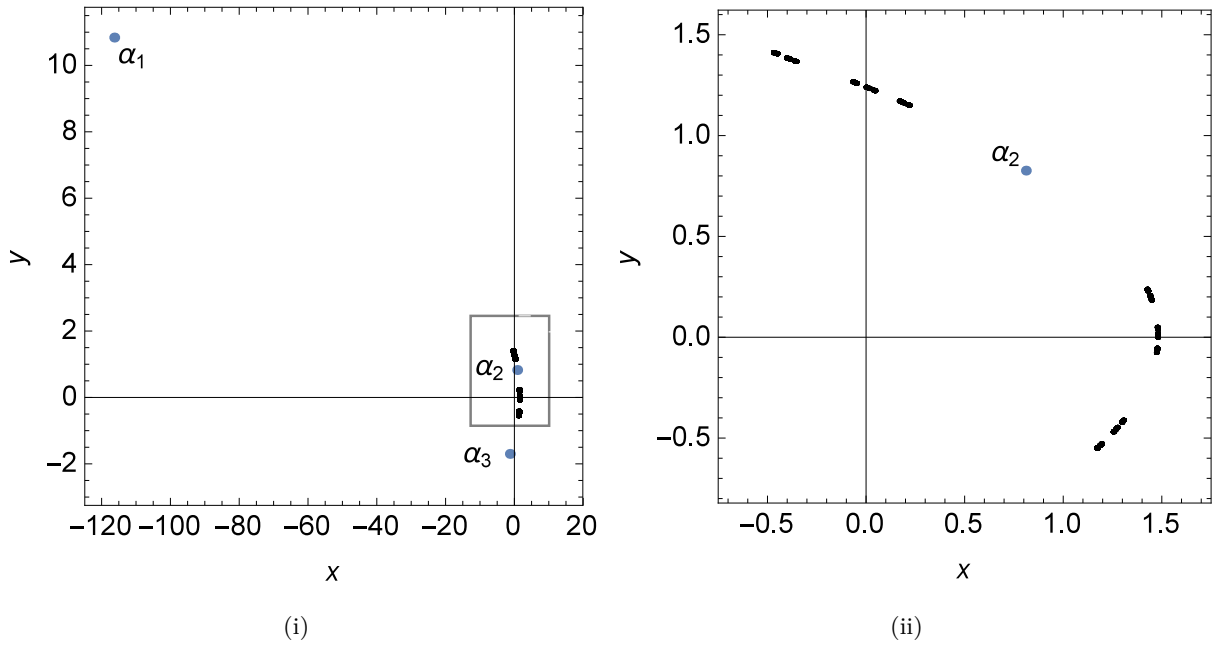

(i) (ii)

Figure 5.4. : (i) The periodic orbits of period 2^{11} (black colour) and the fixed points $\alpha_1, \alpha_2, \alpha_3$ (blue colour) at $\varepsilon = -0.1$ and $b = 0.035$; (ii) zoom part around α_2.

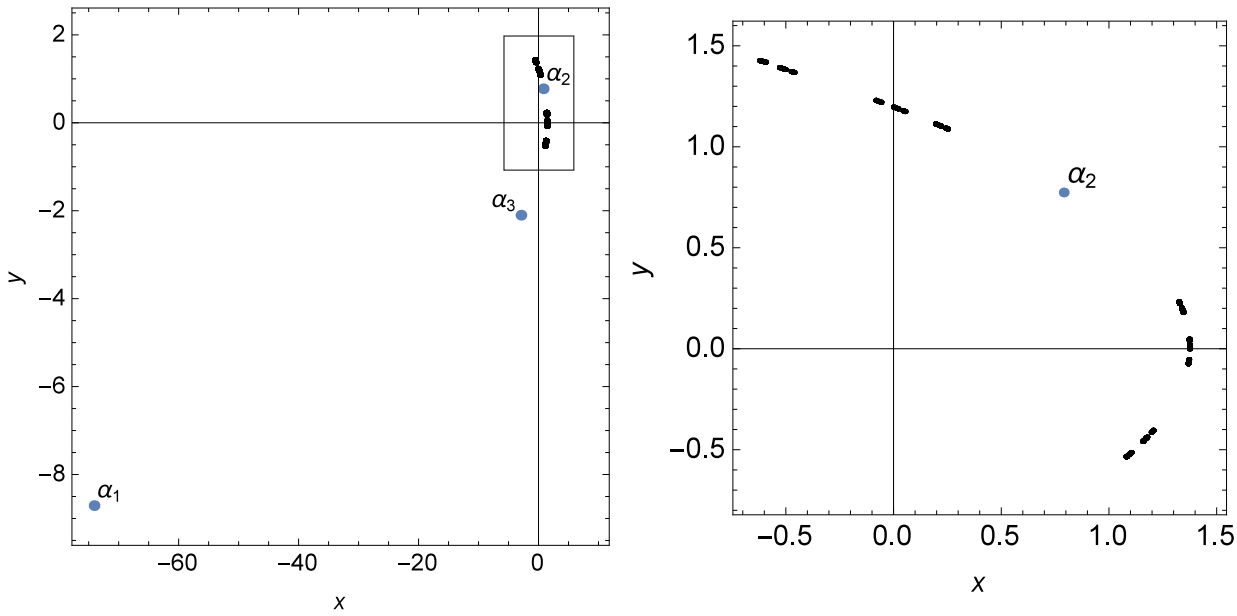

(i) (ii)

Figure 5.5. : (i) The periodic orbits of period 2^{11} (black colour) and the fixed points $\alpha_1, \alpha_2, \alpha_3$ (blue colour) at $\varepsilon = 0.1$ and $b = 0.035$; (ii) zoom part around α_2.

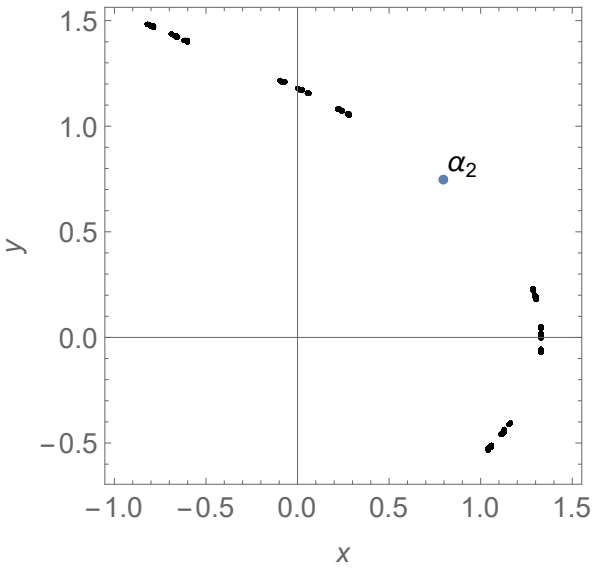

Figure 5.6. : The periodic orbits of period 2^{11} (black colour) and the fixed point α_2 (blue colour) at $\varepsilon = 0.3$ and $b = 0.035$.

We describe the stability of the periodic attractor using the unstable manifolds of fixed points. The unstable manifold of the flip saddle α_2 is denoted by $W^u(\alpha_2)$ and the unstable manifold of regular saddle α_3 is denoted by $W^u(\alpha_3)$, which are plotted in red (thick) and blue (thin) colours respectively. The period-2 points of the map $\mathscr{H}$ are represented by P_{21} and P_{22}. By tracing the

unstable manifold of α_2 around the periodic point P_{22}, we generate a sequence of pictures showing the fact that the unstable manifold of α_2 converges to the period-2 point P_{22}. This is illustrated in Fig. 5.7 and Fig. 5.8 for $\varepsilon = -0.1$ and $\varepsilon = 0.1$ respectively. This dynamics occurs concurrently with the stable fixed point α_1 which describes the presence of coexisting attractor for each $\varepsilon \in \mathscr{D}_\varepsilon^*$. The convergence of the unstable manifold of α_2 to other period-2 point P_{21} are shown in Fig 5.9 and Fig 5.10 of Appendix D for $\varepsilon = -0.1$ and $\varepsilon = 0.1$ respectively. If we further increase ε as $\varepsilon > \varepsilon_*$, such dynamics can not be observed because the two fixed points α_1 and α_3 will disappear and the map has only one fixed point α_2 which is the flip saddle. Note that, in the canonical case $\varepsilon = 0$, the q-Hénon map has two fixed points α_2 and α_3, and the period-2 points P_{21} and P_{22}, both lies on the unstable manifold of α_2.

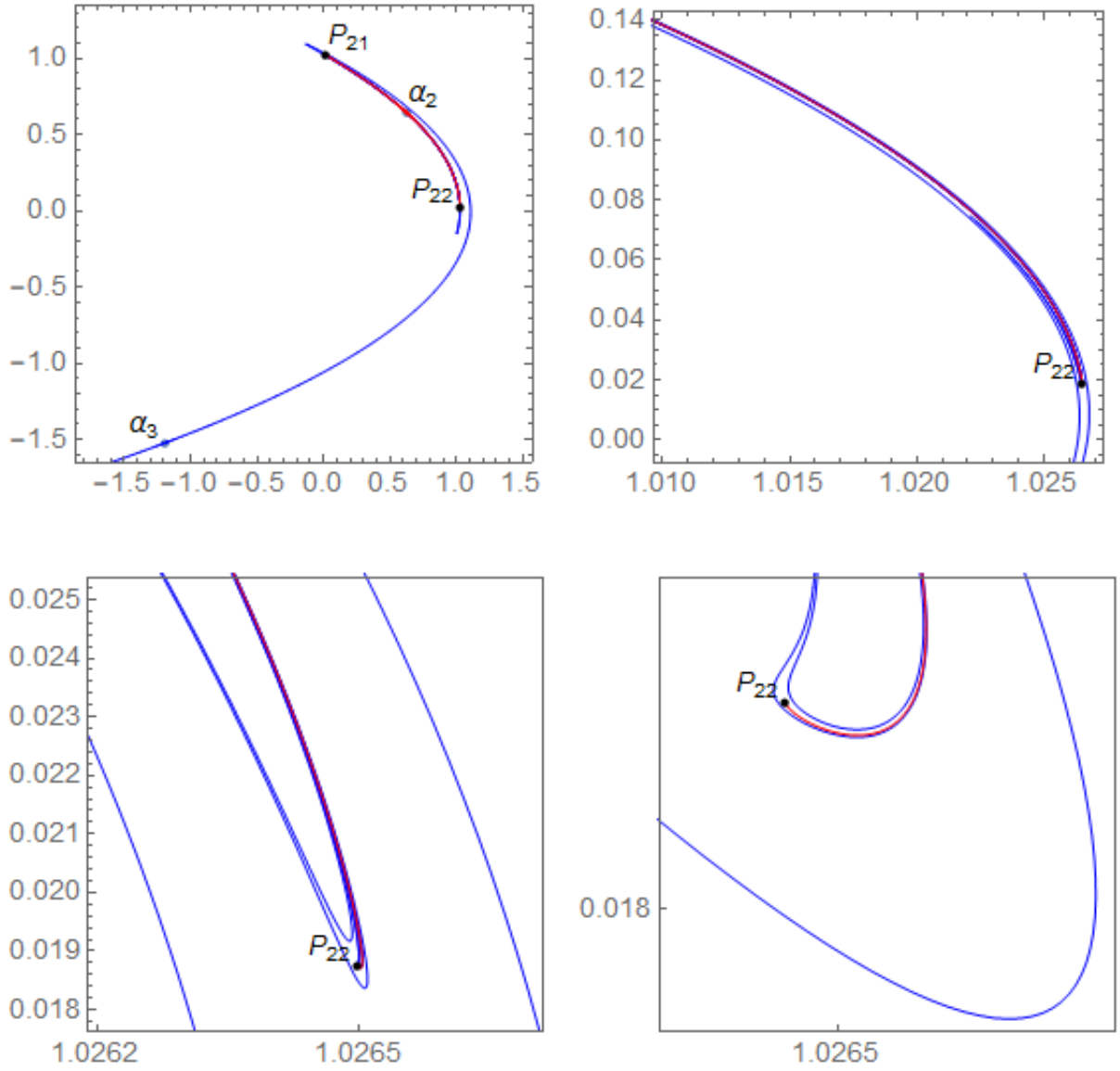

Figure 5.7. : The unstable manifolds $W^u(\alpha_2)$ and $W^u(\alpha_3)$ of $\mathscr{H}_{a,b,\varepsilon}$ are shown by red and blue colours respectively at $\varepsilon = -0.1$ and $b = 0.038$. P_{21} and P_{22} are period 2 orbits.

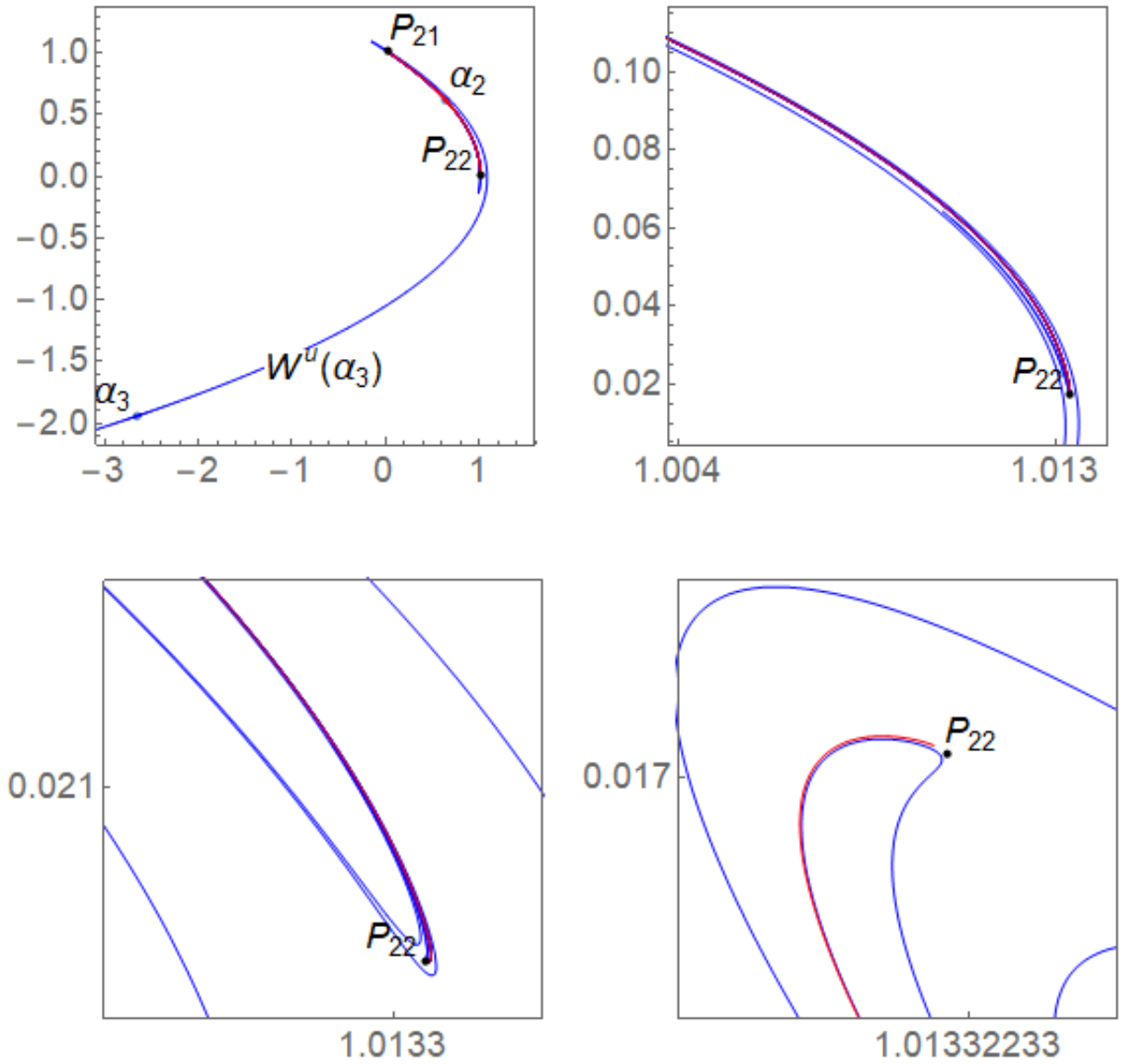

Figure 5.8. : The unstable manifolds $W^u(\alpha_2)$ and $W^u(\alpha_3)$ of $\mathscr{H}_{a,b,\varepsilon}$ are shown by red and blue colours respectively at $\varepsilon = 0.1$ and $b = 0.035$; P_{21} and P_{22} are period 2 orbits.

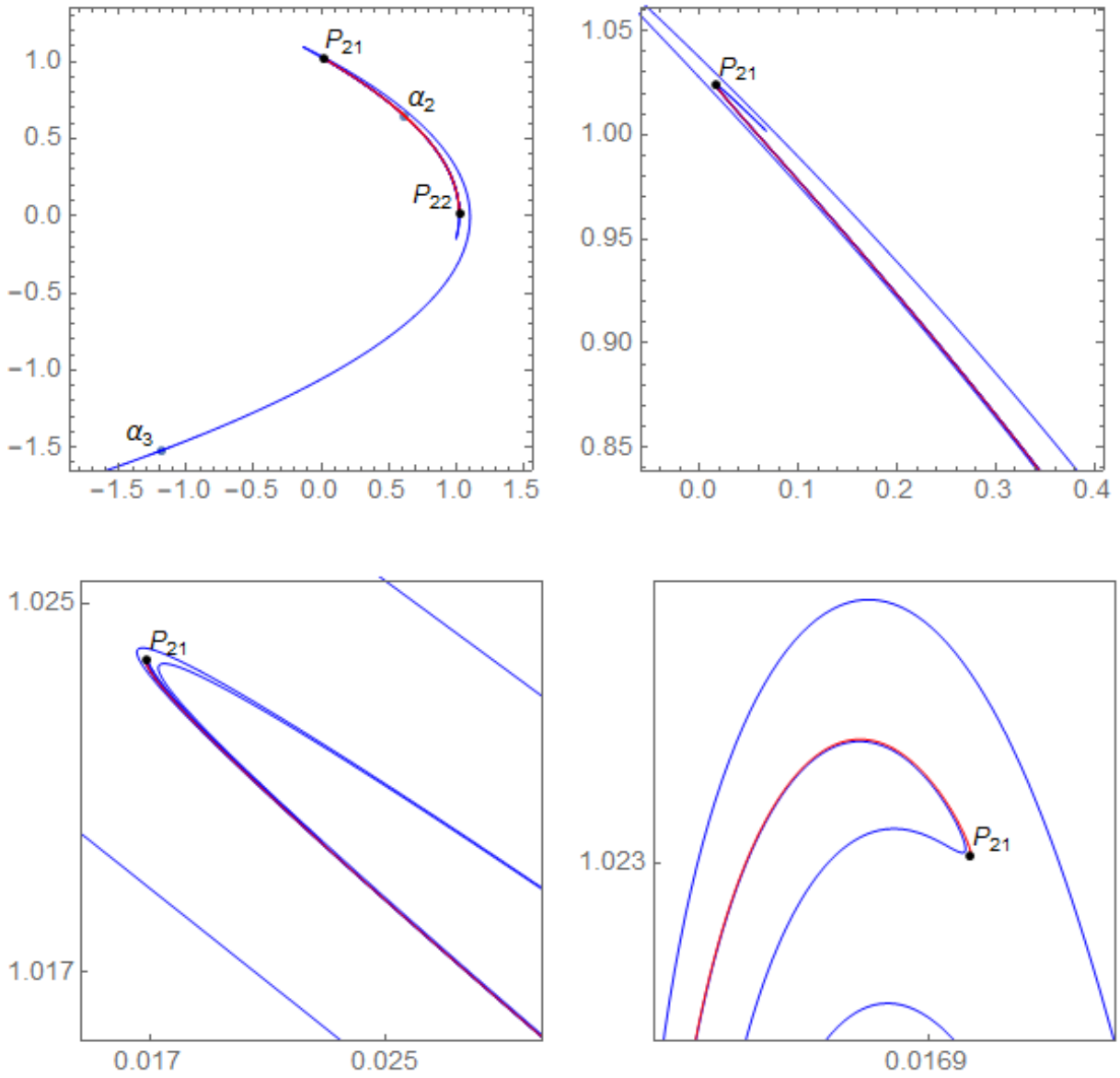

Figure 5.9. : Unstable manifolds of the fixed points α_2 and α_3 shown by red and blue colours respectively for $\varepsilon = -0.1$ and $b = 0.038$, black dots are period-2 orbits.

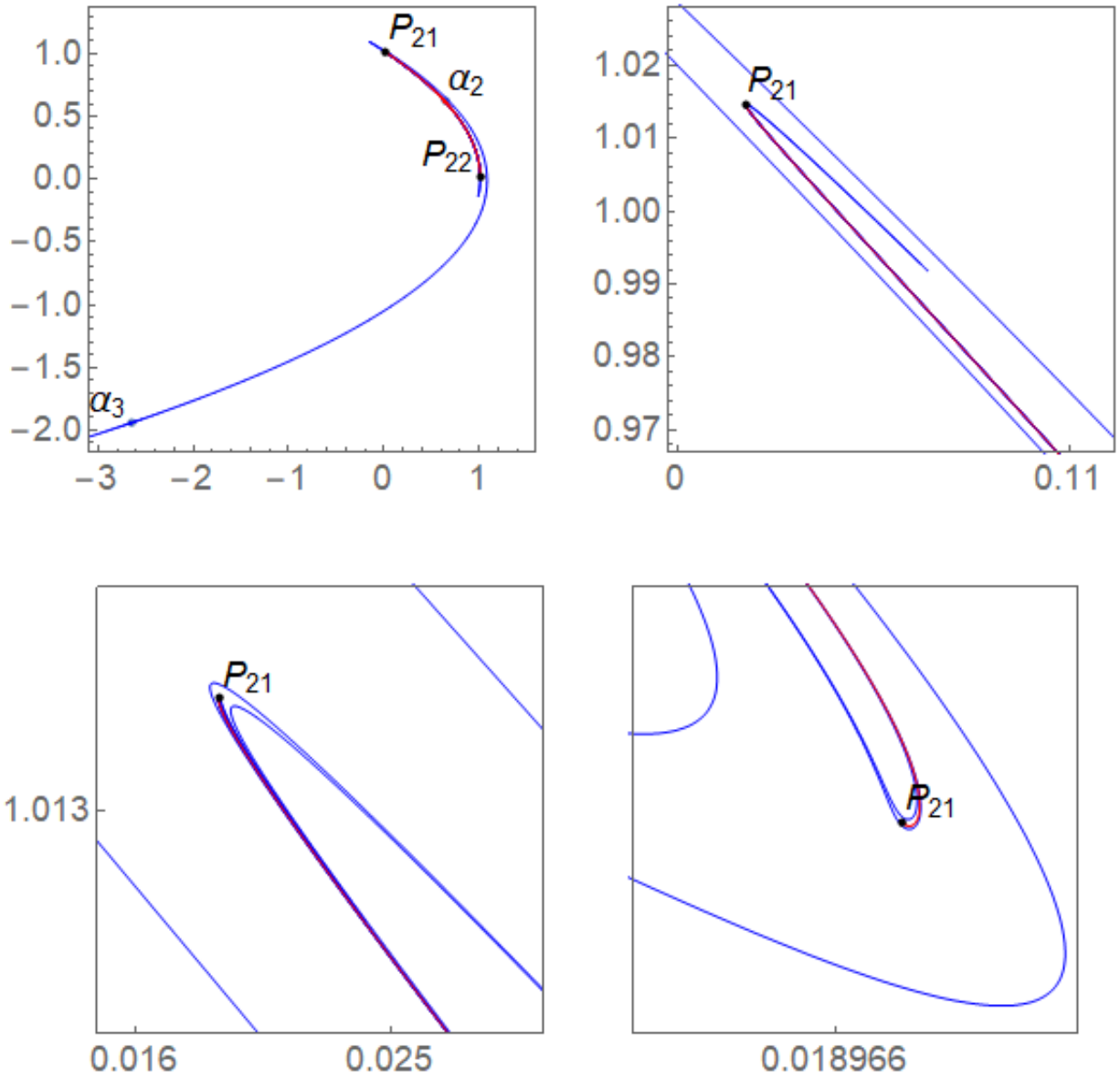

Figure 5.10. : Unstable manifolds of the fixed points α_2 and α_3 shown by red and blue colours respectively for $\varepsilon = 0.1$ and $b = 0.035$, black dots are period-2 orbits.

5.4 HETEROCLINIC WEB AND RENORMALIZABLE MAPS

Let $\mathscr{H}_{a,b,\varepsilon}$ be a q-Hénon map on the curve $\gamma_{2^n,\varepsilon}$ with $\varepsilon \in \mathscr{D}_\varepsilon^*$, where $\mathscr{D}_\varepsilon^* = (-0.2, \varepsilon_*) \setminus \{0\}$.

Definition 5.4.1. *Heteroclinic Web: The structure of unstable manifold of regular saddle α_3 and stable manifold of flip saddle α_2 is called heteroclinic web.*

Definition 5.4.2. *Heteroclinic Tangency: We say the map $\mathscr{H}_{a,b,\varepsilon}$ has heteroclinic tangency, if there exists a parameter b_* on $\gamma_{2^n,\varepsilon}$, such that the unstable manifold of α_3 touches the stable manifold of α_2 at some point s_0. At this point s_0, the local unstable manifold of α_3 has the shape of unimodal map. Further, the map $\mathscr{H}_{a,b,\varepsilon}$ undergoes heteroclinic bifurcation at b_*. This is illustrated for a particular map, which is shown in Fig. 5.11.*

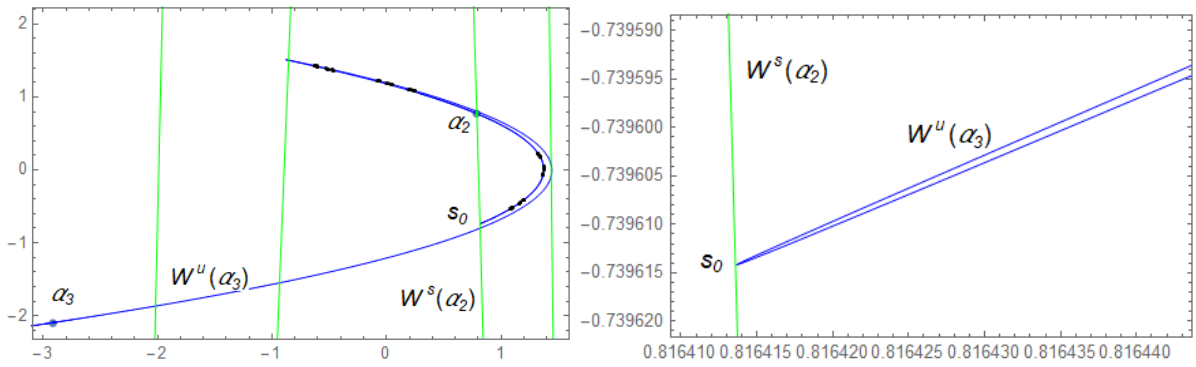

(i) (ii)

Figure 5.11. : (i) Bifurcation moment of q-Hénon map at $b_* = 0.03000426$ on $\gamma_{2^n,\varepsilon}$ for $\varepsilon = 0.1$ and 2^8 period; (ii) Magnification around the point s_0, where $W^u(\alpha_3)$ touches $W^s(\alpha_2)$.

We use the following algorithm to compute the heteroclinic bifurcation on the curve $\gamma_{2^n,\varepsilon}$.

1. For $\varepsilon \in \mathscr{D}_\varepsilon^*$, we have the parameters (a,b) on the curve $\gamma_{2^n,\varepsilon}$ such that the map $\mathscr{H}_{a,b,\varepsilon}$ has a strongly attracting periodic orbit of period 2^n.

2. For each $b \in [0, 0.05]$ on the curve $\gamma_{2^n,\varepsilon}$, we calculate the fixed points α_1, α_2 and α_3, and subsequently plot the heteroclinic web.

3. As we vary b value, one can observe that there exist b_* such that the heteroclinic web of $\mathscr{H}_{a,b_*,\varepsilon}$ has heteroclinic tangency. In other words, at that parameter b_*, the map undergoes heteroclinic bifurcation.

4. Repeat the Step 1 to 3 to calculate the parameter b_* corresponding to the heteroclinic bifurcation, for different ε value.

By using the above steps we have computed the heteroclinic bifurcation of q-Hénon map on the curve $\gamma_{2^n,\varepsilon}$, when $\varepsilon = 0.1$ and obtained $b_* = 0.03000426$. It is shown in the Fig. 5.11. Further, the heteroclinic bifurcation b_* for different curves $\gamma_{2^n,\varepsilon}$ associated with ε are computed and shown in Table 5.2. We observe that the value of b_* decreases as ε increases from -0.1 to 0.15. When $\varepsilon > \varepsilon_*$ the maps on the curve $\gamma_{2^n,\varepsilon}$ have only one fixed point and therefore the heteroclinic bifurcation do not occur.

ε	**Heteroclinic bifurcation** b_*
-0.1	0.03237592
0	0.03095192
0.05	0.03043535
0.1	0.03000426
0.15	0.02964028

Table 5.2. : Heteroclinic bifurcation for different ε.

Now, we give the topological definition of renormalization of q-Hénon map, which is inspired from the work related to the renormalization of dissipative Hénon-like maps in [De Carvalho *et al.*, 2005], [Lyubich and Martens, 2011], [Chandramouli, 2008].

Definition 5.4.3. *The q-Hénon map $\mathscr{H}_{a,b,\varepsilon}$ is said to be renormalizable if there are three fixed points, in which one is stable, one is flip saddle, and other one is regular saddle such that the unstable manifold of regular saddle intersects the stable manifold of flip saddle in a single orbit.*

Definition 5.4.4. *The q-Hénon map $\mathscr{H}$ is said to be n^{th}-Renormalizable if*

(i). The local unstable manifold of $P_{2^{n-2}}$ is denoted by $W^u_{loc}(P_{2^{n-2}})$ intersects the local stable manifold of $P_{2^{n-1}}$ is denoted by $W^s_{loc}(P_{2^{n-1}})$ in a single orbit, where $n \geq 2$. The points P_{2^i} are saddle points of period 2^i for $i \geq 1$ and $P_1 = \alpha_2$.

(ii). A piece of $W^u_{loc}(P_{2^{n-2}})$ and a piece of $W^s_{loc}(P_{2^{n-1}})$ form a disk D_n such that D_n is invariant under $\mathscr{H}^{2^n}$.

(iii). $int(\mathscr{H}^i(D_n))$ are piecewise disjoint for $i = 0, 1, \ldots 2^{n-1}$.

The first renormalization of the map $\mathscr{H}_{a,b,\varepsilon}$ on the curve $\gamma_{2^n,\varepsilon}$ is illustrated in the Fig. 5.12 by considering parameters $\varepsilon = 0.1$ and $b = 0.01499$. In which, $W^s_{loc}(\alpha_2)$ intersects $W^u_{loc}(\alpha_3)$ in a single orbit. The second renormalization is shown in the Fig. 5.13, where $W^u_{loc}(\alpha_2)$ intersects $W^s_{loc}(P_2)$ in a single orbit. Here, $W^s_{loc}(P_2)$ is the stable manifold of period-2 point P_2.

Let $\widetilde{\gamma}_{2^n,\varepsilon}$ be a graph over $[0, b_*]$ such that it is a subcurve of the $\gamma_{2^n,\varepsilon}$. Clearly, from the Definition 5.4.4, the map $\mathscr{H}_{a,b,\varepsilon}$ is $n-$times renormalizable on the curve $\widetilde{\gamma}_{2^n,\varepsilon}$. Therefore, as $n \to \infty$, the map $\mathscr{H}_{a,b,\varepsilon}$ on the curve $\widetilde{\gamma}_{2^\infty,\varepsilon}$ is infinitely renormalizable for every $\varepsilon \in \mathscr{D}^*_\varepsilon$. From the work of [De Carvalho *et al.*, 2005], we conclude that the map $\mathscr{H}_{a,b,\varepsilon}$ has a Cantor attractor $\mathscr{O}_{\mathscr{H}}$ and a collection of disks $D_1 \supset D_2 \supset D_3 \ldots D_n$ such that

- $D_k \supset \mathscr{H}^{2^k}(D_k)$.
- $\mathscr{H}^i(D_n) \cap \mathscr{H}^j(D_n) \neq \emptyset$ for $i \neq j$ and $i, j \leq 2^k$.
- The disks D_k are bounded by a local unstable manifold of $P_{2^{k-2}}$ and a local stable manifold $P_{2^{k-1}}$, where the points P_{2^i} are saddle points of period 2^i for $i \geq 1$ and $P_1 = \alpha_2$.

The orbit of D_n are denoted by $\mathscr{C}_n$, where

$$\mathscr{C}_n = \{D_n, \mathscr{H}(D_n), \mathscr{H}^2(D_n) \ldots \mathscr{H}^{2^{n-1}}(D_n)\}.$$

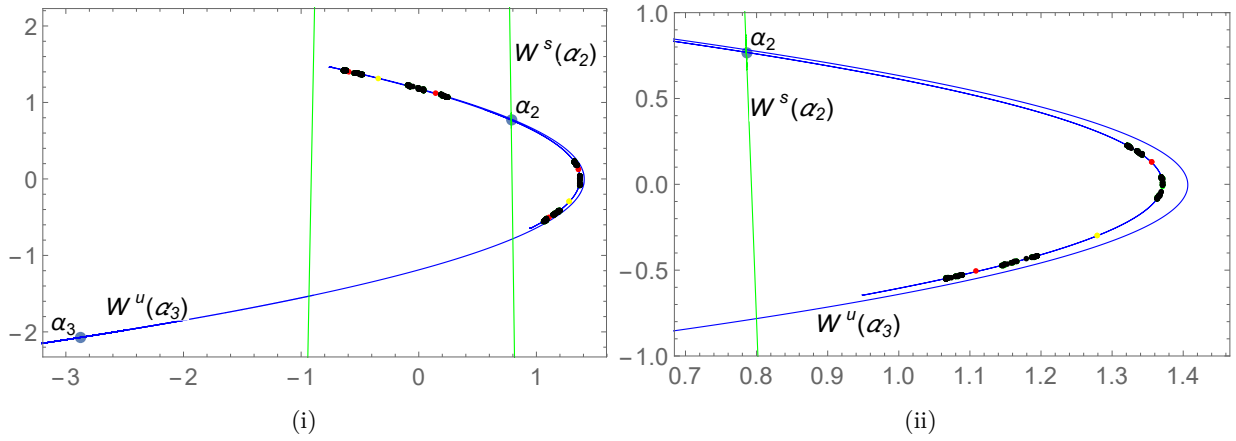

Figure 5.12. : (i) First renormalization of $\mathscr{H}_{a,b,\varepsilon}$ on $\gamma_{2^8,\varepsilon}$ for $\varepsilon = 0.1$ at $b = 0.01499$; $W^s(\alpha_2)$ is the stable manifold of α_2 and $W^u(\alpha_3)$ is the unstable manifold of α_3; (ii) Zoom part around α_2.

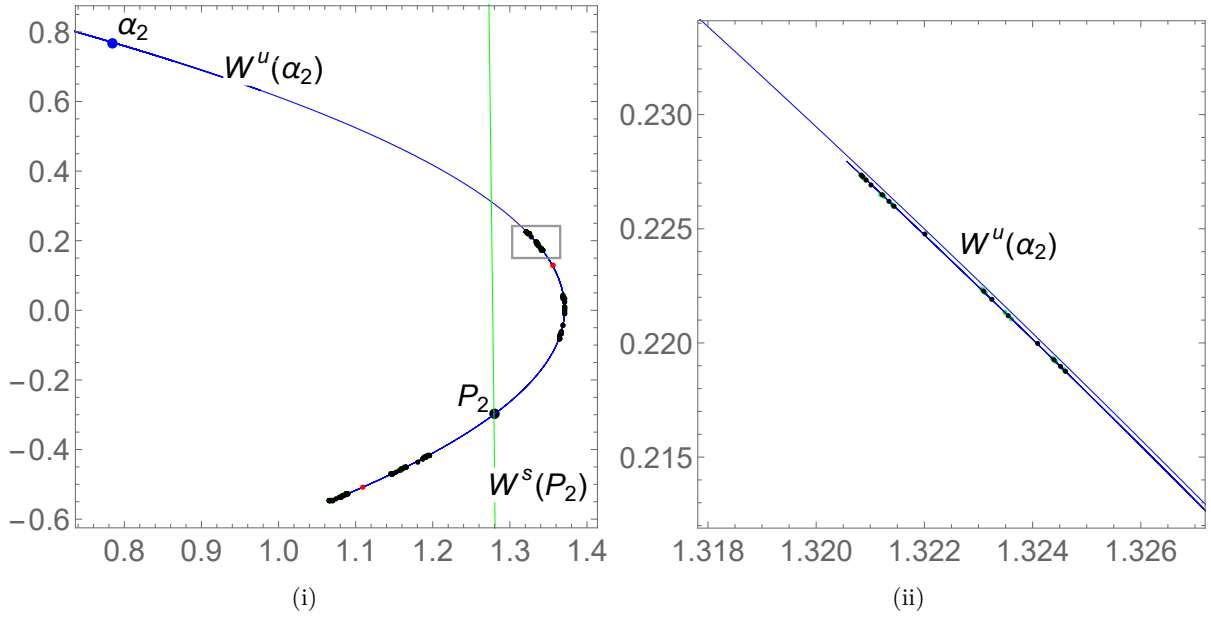

Figure 5.13. : (i) Second renormalization of $\mathscr{H}_{a,b,\varepsilon}$ on $\gamma_{2^8,\varepsilon}$ for $\varepsilon = 0.1$ and $b = 0.01499$; $W^u(\alpha_2)$ is the unstable manifold of fixed point α_2 and $W^s(P_2)$ is the stable manifold of period 2 point P_2; (ii) Zoom part.

This is referred as n^{th} cycle. Therefore the Cantor set $\mathscr{O}_{\mathscr{H}}$ is

$$\mathscr{O}_{\mathscr{H}} = \bigcap_{n\geq 1} \bigcup_{i=0}^{2^n-1} \mathscr{H}^i(D_n).$$

So the Cantor set $\mathscr{O}_{\mathscr{H}}$ formed such that

$$\mathscr{C}_1 \supset \mathscr{C}_2 \supset \mathscr{C}_3 \supset \ldots \mathscr{C}_n \supset \ldots \mathscr{O}_{\mathscr{H}}.$$

Then we have the following proposition:

Proposition 5.4.5. *Let $\mathscr{H}_{a,b,\varepsilon}$ be any q-Hénon map with $(a,b) \in \gamma_{2^\infty,\varepsilon}$ and $\varepsilon \in \mathscr{D}_\varepsilon^*$, then we have $\mathscr{H}_{a,b,\varepsilon}$ is infinitely renormalizable. In particular, $\mathscr{O}_{\mathscr{H}}$ is a Cantor attractor.*

Remark 5.4.6. *The map $\mathscr{H}_{a,b,\varepsilon}$ is infinitely renormalizable only for $\varepsilon \in \mathscr{D}_\varepsilon^*$ but it fails for $\varepsilon > \varepsilon_*$.*

5.5 BASIN OF ATTRACTION

The collection of all initial conditions in the phase space whose trajectories leads to the attracting set is called basin of attraction of the set. The basin of attraction can also be a point at infinity (in the sense that some initial conditions escape to infinity). We investigate the changes in the basin of attraction of the maps $\mathscr{H}_{a,b,\varepsilon}$ on the curve $\gamma_{2^n,\varepsilon}$. For $\varepsilon \in \mathscr{D}_\varepsilon^*$, we know that the q-Hénon maps have superstable periodic attractor of period 2^n and a coexisting fixed point α_1. Therefore one can compute the approximation of basin of attraction.

Let $B = \{(x,y) : -l \le x \le l; -br \le y \le br\}$ be the domain such that the fixed points α_2 and α_3 lie within the domain B. Suppose M is a grid of $m \times n$ mesh points in B such that $M = \{(x_i, y_j) : x_i \in [-l,l]; y_j \in [-br, br] \; \forall \, 1 \le i \le m; \, 1 \le j \le n\}$. We compute the basin of attraction of the map $\mathscr{H}_{a,b,\varepsilon}$ by iterating each mesh point. If the orbit of (x_i, y_j) leave the box B in a finite number of iterates then we say that trajectory of (x_i, y_j) is escaping to infinity. In this case, we mark this point (x_i, y_j) with red colour. If the orbit of (x_i, y_j) converges to the periodic attractor of period 2^n, then mark (x_i, y_j) as a blue colour otherwise the orbit of (x_i, y_j) converges to coexisting fixed point α_1 then mark it as a yellow colour. Note that the basin of attraction of the map does not cover the whole plane and the reason is that most of initial conditions that are far from the attractor, either converge to a coexisting fixed point or approaches to infinity.

The basin of attraction of $\mathscr{H}_{a,b,\varepsilon}$ for $b = 0.0499\ldots$ is shown in Fig. 5.14 for various ε values. The blue region indicates the basin of periodic attractor of period 2^n, the yellow region indicates the basin of coexisting fixed point α_1 and the red colour represents the escaping region, where the black points in the blue region indicates the periodic attractor. From the Fig. 5.14(i) and Fig. 5.14(ii), we observe that the basin of $\mathscr{H}_{a,b,\varepsilon}$ contain three regions including the basin corresponding to the periodic attractor, coexisting attractor α_1 and escaping region. When $\varepsilon = 0$, it is the case of canonical Hénon-like map and therefore the basin contains only attracting region and escaping region, which is shown in Fig. 5.14(iii).

For $\varepsilon \in (0, \varepsilon_*)$, the basin of $\mathscr{H}_{a,b,\varepsilon}$ do not contain the escaping region. It contains only two regions, one is converging to the periodic attractor and other is converging to α_1, it is illustrated in Fig. 5.14(iv) and Fig. 5.14(v). This is an interesting phenomenon similar to the Lorenz system. To further illustrate the basin of attraction in the region $\varepsilon \in (0, \varepsilon_*)$, we plotted the basin of attraction for different $b \in (0, 0.05)$ by choosing $\varepsilon = 0.05$ and $\varepsilon = 0.15$, which are depicted in Fig.5.15 and Fig.5.16 respectively.

For $\varepsilon > \varepsilon_*$, the map $\mathscr{H}_{a,b,\varepsilon}$ do not have the coexisting fixed point, therefore the basin of attraction has two regions, in which one is attracting towards periodic attractor and other one is escaping to infinity. It is shown in Fig. 5.14(vi).

5.6 CONCLUSIONS

In this chapter, we have investigated the dynamical properties of q-Hénon map $\mathscr{H}_{a,b,\varepsilon}$ which has a non-constant Jacobian. We proposed a method for computing the superstable periodic orbits of the q-Hénon map on the parameter space for different deformed parameters. Using this, we have constructed the "most attracting curve" denoted by $\gamma_{2^n,\varepsilon}$ on the parameter space. As $n \to \infty$, on the

curve $\gamma_{2^\infty,\varepsilon}$, the phase transition take place from simple to chaotic dynamics. We observed that as the deformed parameter ε increases, the system become chaotic in the wide range of the parameter space a. When $\varepsilon > 0$, the Parrondo's paradox is encountered for the q-Hénon maps $\mathscr{H}_{a,b,\varepsilon}$, as the phase transition occurs earlier than the canonical Hénon-like map $H_{a,b}$. We also described the location of the periodic attractor by tracing the stable and unstable manifolds of fixed points.

We discussed the concept of heteroclinic web, which is based on the structure of stable and unstable manifolds of saddle periodic points. Varying b value on each $\gamma_{2^n,\varepsilon}$, we computed the heteroclinic bifurcations using the heteroclinic web. We showed that for each $\varepsilon \in \mathscr{D}_\varepsilon^*$ on the curve $\widetilde{\gamma}_{2^\infty,\varepsilon}$, all q-Hénon maps are infinitely renormalizable and having Cantor set as an attractor. Finally, we have computed the basin of attraction of q-Hénon maps and observed that the q-Hénon map do not have an escaping region for each $\varepsilon \in (0, \varepsilon^*)$. This is an interesting property, which shows the similarity of q-Hénon map with Lorenz system in which all trajectories are bounded.

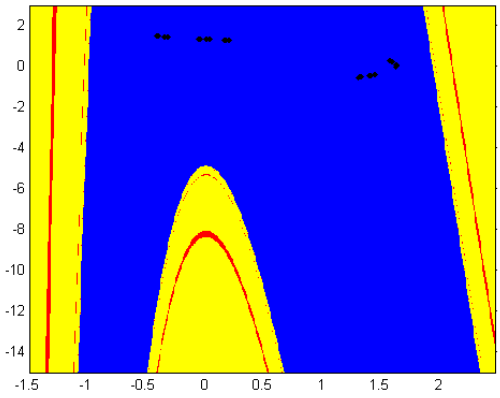

(i) $\varepsilon = -0.2$

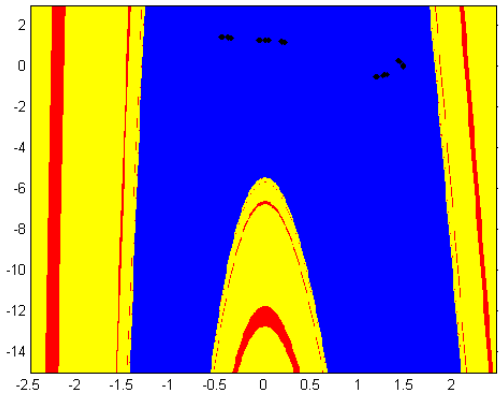

(ii) $\varepsilon = -0.1$

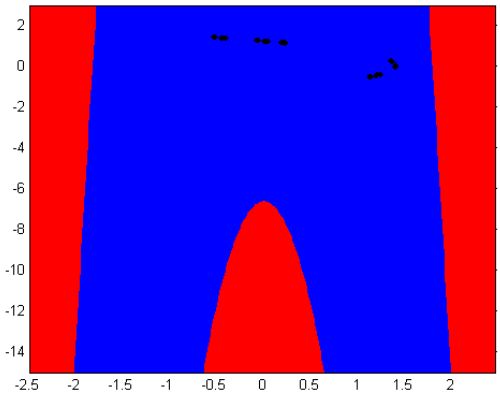

(iii) $\varepsilon = 0$

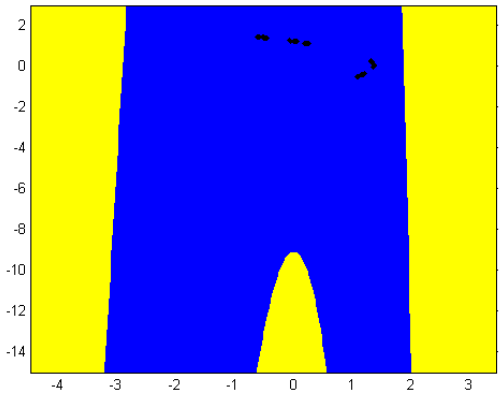

(iv) $\varepsilon = 0.1$

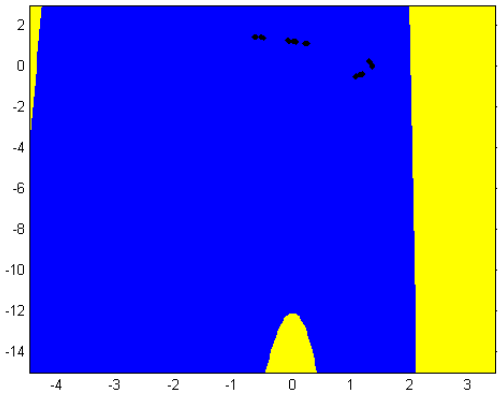

(v) $\varepsilon = 0.15$

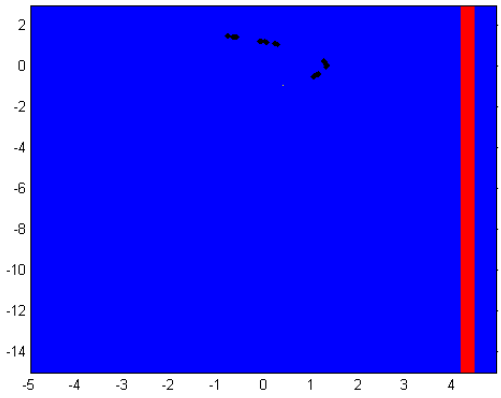

(vi) $\varepsilon = 0.3$

Figure 5.14. : Basin of attraction of q-Hénon map for period 256 and for different ε, where b=0.04999 and (i) $a = 1.705320951200358$; (ii) $a = 1.550975058042254$; (iii) $a = 1.478456522436630$; (iv) $a = 1.436441173331582$; (v) $a = 1.421663539980441$; (vi) $a = 1.391750276903475$.

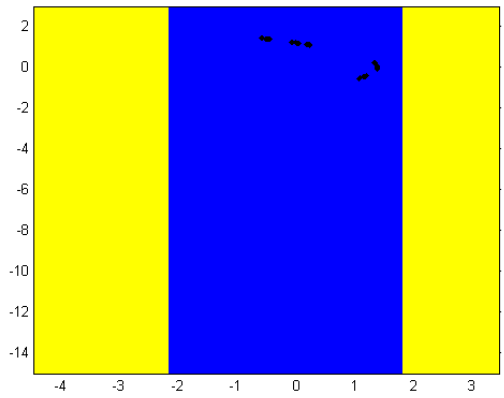

(i) $b = 0$

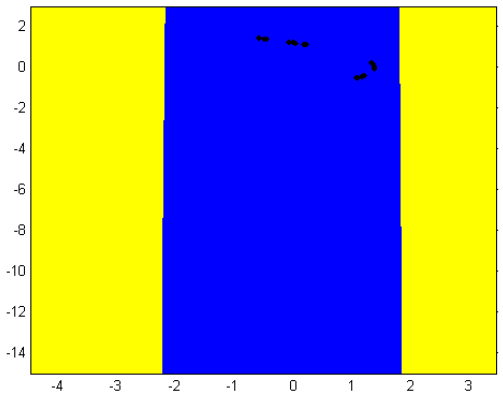

(ii) $b = 0.01$

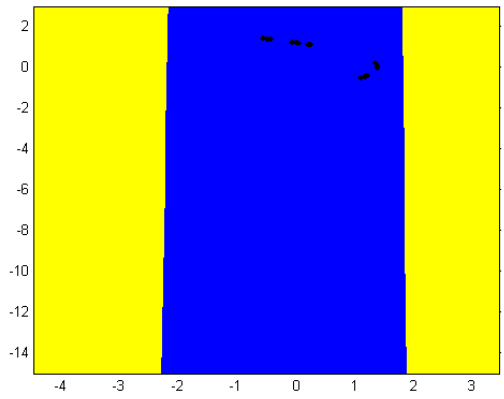

(iii) $b = 0.02$

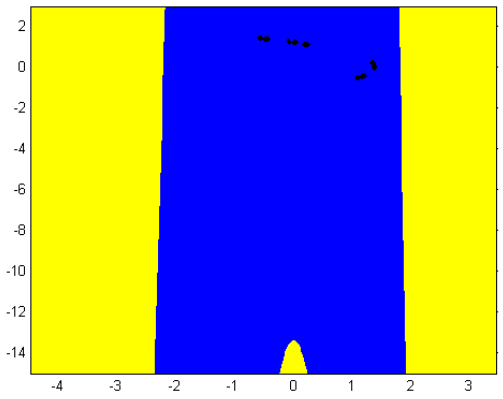

(iv) $b = 0.03$

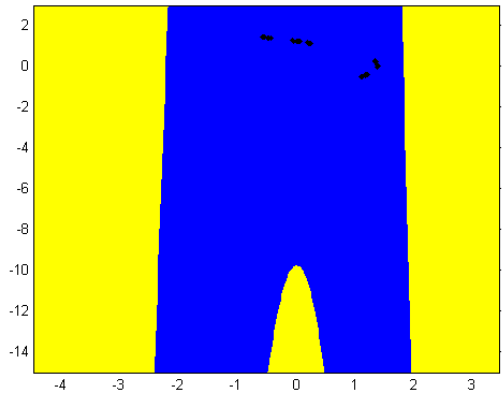

(v) $b = 0.04$

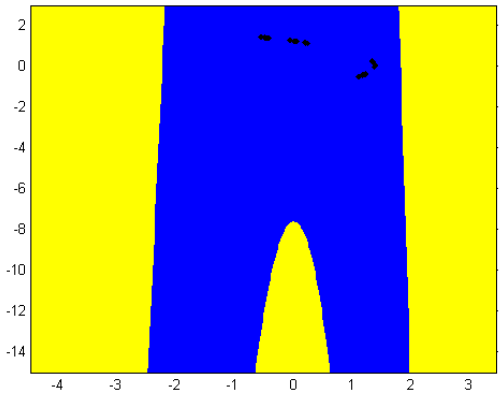

(vi) $b = 0.05$

Figure 5.15. : Basin of attraction of q-Hénon map for period 256 and for different b at $\varepsilon = 0.05$.

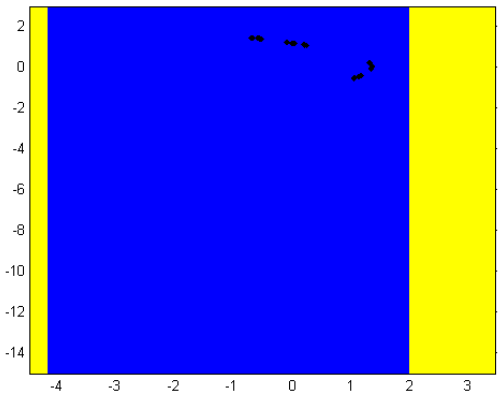

(i) $b = 0$

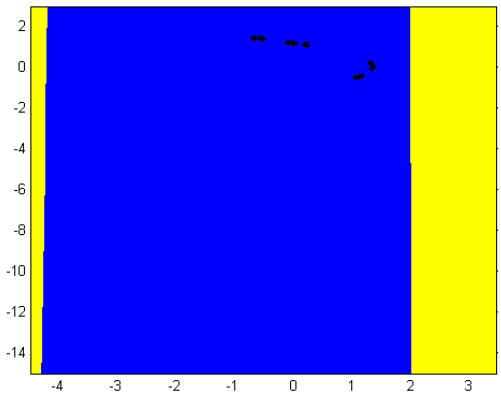

(ii) $b = 0.01$

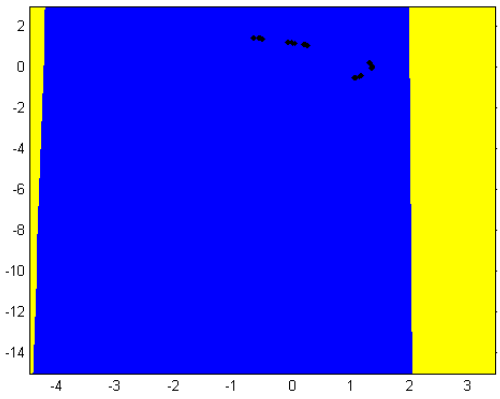

(iii) $b = 0.02$

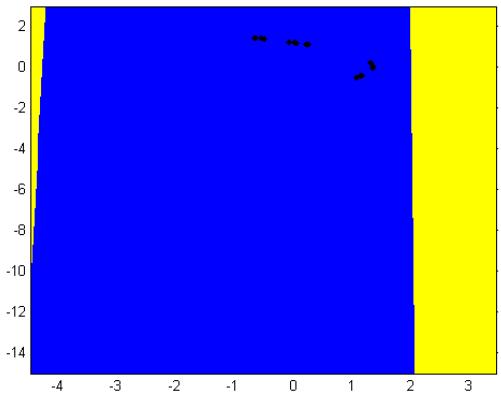

(iv) $b = 0.03$

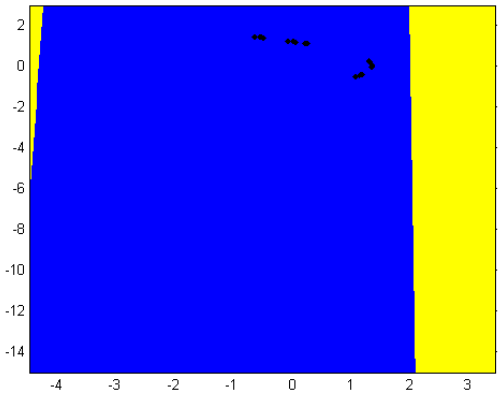

(v) $b = 0.04$

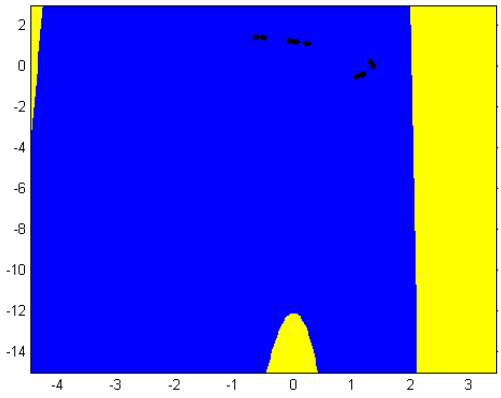

(vi) $b = 0.05$

Figure 5.16. : Basin of attraction of q-Hénon map for period 256 and for different b at $\varepsilon = 0.15$.